



City Research Online

City, University of London Institutional Repository

Citation: Zhang, H., Zhou, L., Xu, J., Wang, N., Hu, H., Lu, L., Rahman, B. M. & Chen, J. (2019). Nonvolatile waveguide transmission tuning with electrically-driven ultra-small GST phase-change material. *Science Bulletin*, 64(11), pp. 782-789. doi: 10.1016/j.scib.2019.04.035

This is the published version of the paper.

This version of the publication may differ from the final published version.

Permanent repository link: <https://openaccess.city.ac.uk/id/eprint/22618/>

Link to published version: <https://doi.org/10.1016/j.scib.2019.04.035>

Copyright: City Research Online aims to make research outputs of City, University of London available to a wider audience. Copyright and Moral Rights remain with the author(s) and/or copyright holders. URLs from City Research Online may be freely distributed and linked to.

Reuse: Copies of full items can be used for personal research or study, educational, or not-for-profit purposes without prior permission or charge. Provided that the authors, title and full bibliographic details are credited, a hyperlink and/or URL is given for the original metadata page and the content is not changed in any way.

City Research Online:

<http://openaccess.city.ac.uk/>

publications@city.ac.uk



Article

Nonvolatile waveguide transmission tuning with electrically-driven ultra-small GST phase-change material

Hanyu Zhang^a, Linjie Zhou^{a,*}, Jian Xu^a, Ningning Wang^a, Hao Hu^a, Liangjun Lu^a, B. M. A. Rahman^b, Jianping Chen^a

^aState Key Laboratory of Advanced Optical Communication Systems and Networks, Shanghai Key Laboratory of Navigation and Location Services, Shanghai Institute for Advanced Communication and Data Science, Department of Electronic Engineering, Shanghai Jiao Tong University, Shanghai 200240, China

^bDepartment of Electrical and Electronic Engineering, City, University of London, London EC 1V 0HB, UK

ARTICLE INFO

Article history:

Received 10 February 2019

Received in revised form 16 April 2019

Accepted 29 April 2019

Available online 3 May 2019

Keywords:

Phase change material

Nonvolatile optical switch

Integrated optics devices

Chalcogenide Ge₂Sb₂Te₅

ABSTRACT

Low-power reconfigurable optical circuits are highly demanded to satisfy a variety of different applications. Conventional electro-optic and thermo-optic refractive index tuning methods in silicon photonics are not suitable for reconfiguration of optical circuits due to their high static power consumption and volatility. We propose and demonstrate a nonvolatile tuning method by utilizing the reversible phase change property of GST integrated on top of the silicon waveguide. The phase change is enabled by applying electrical pulses to the μm -sized GST active region in a sandwich structure. The experimental results show that the optical transmission of the silicon waveguide can be tuned by controlling the phase state of GST.

© 2019 Science China Press. Published by Elsevier B.V. and Science China Press. This is an open access article under the CC BY license (<http://creativecommons.org/licenses/by/4.0/>).

1. Introduction

Photonic integration is a development trend for optical systems that are widely used in various optical interconnection and signal processing systems [1–3]. Similar to the application-specific integrated circuits (ASICs), a photonic integrated circuit can also be designed to satisfy a specific application where a particular function is performed with a fixed optical circuit configuration [4,5]. Although the performance can be well optimized after multiple rounds of design and fabrication iterations, the lack of versatility makes it impossible to become a general low-cost solution to various price-sensitive applications. Therefore, programmable optical circuits are in high demand for general purposes, where different functions can be provided by simply resetting several key components [6].

Waveguide refractive index (RI) tuning is the basis for actively tunable devices. In silicon photonics, thermo-optic (TO) and electro-optic (EO) effects are routinely used for RI tuning, but they are both volatile and require a continuous power supply to maintain the states. This leads to large static power consumption, especially for reconfigurable optical circuits, like optical circuit switches [7] and optical signal processors [8,9] when the optical paths are not frequently changed.

One solution for nonvolatile RI tuning is to integrate phase change material (PCM) with silicon [10,11]. The PCM has a dramatic change in the optical property after phase transition between amorphous and crystalline states [12]. It is possible to obtain a large RI change of $\Delta n > 1$. Moreover, because of the stable phases, the tuned RI can be kept for a long time without power consumption. This property makes it quite attractive for reconfigurable optical circuits. Ge₂Sb₂Te₅ (GST) is a classical chalcogenide alloy in which the phase change can be actuated either by thermal, optical or electrical stimulations potentially with an ultrahigh speed [13–17].

In recent years, there has been increased interest in GST for photonic devices. A lot of exciting works have been done in photonic devices for applications targeted for neuromorphic computing, multi-level storage, display, optical switches [18–20], and photonic in-memory computing [21–25]. The optical switch can be based on a multimode interferometer (MMI) loaded with GST and the phase change is enabled by light pulse irradiation from an out-of-plane laser [18]. However, it is quite challenging to apply this method to a large-scale photonic integrated circuit. An integrated all-photonic non-volatile multi-level memory has been demonstrated [24]. The phase change is induced by pump pulses from an in-plane waveguide. This method improves the integration capability, suitable for all-optical signal processing.

In this work, we investigate nonvolatile optical transmission adjustment in a silicon waveguide integrated with a μm -sized

* Corresponding author.

E-mail address: ljzhou@sjtu.edu.cn (L. Zhou).

GST. The GST is sandwiched between two electrodes made of a highly-doped silicon layer and an ITO layer. The active tuning is realized by applying electrical pulses to the GST to raise the temperature high enough to induce phase change. Using electrical signals to control the optical wave is highly demanded in electrically reconfigurable photonic circuits.

2. Device design and simulation

Fig. 1a shows the entire structure of the device. A regular silicon strip waveguide with a width of 500 nm and a height of 220 nm is inserted with a 1 × 1 MMI-based waveguide crossing. The MMI has a length of 12 μm and a width of 2 μm. The waveguides are connected to the MMI through 4-μm-long tapers. The MMI crossing serves for two purposes. First, based on the self-imaging principle, the input light will be focused to the center of the MMI with a reduced divergence angle. Therefore, light can go through the MMI crossing with a low insertion loss. Second, the electrodes are placed on top of the silicon pads that are orthogonally oriented with respect to the waveguide so that optical transmission through the MMI crossing can be electrically controlled.

The inset of Fig. 1a shows the detailed structure of the MMI crossing. The P⁺⁺-doped silicon region is overlapped with the GST/ITO stack on top of the MMI crossing. The overlapped region is a circular disk with an area of π × (D_{GST}/2)². Electrical pulses from the P⁺⁺-doped silicon go through the GST film and arrive at the ITO, causing ohmic heating and therefore inducing phase change. The ITO layer also protects the GST from being oxidized when exposed in the air. The GST/ITO layer thickness is 40 nm/40 nm.

To reset the GST from the crystalline phase to the amorphous phase, the GST is first melted and then quenched rapidly by applying a high-voltage electrical pulse for a short time period. To set the GST film back to the crystalline state, a medium-voltage electrical pulse is applied to anneal the active region at a temperature between the crystallization temperature and the melting temperature for a time period long enough to crystallize GST. In this way, we are able to switch the material between its amorphous (low absorption) and crystalline (high absorption) states in a non-volatile manner. Finite-difference time-domain (FDTD) simulations were performed to calculate the light propagation through the MMI crossing. Fig. 1b shows the cross-sectional electrical-field intensity (|E|²) distributions in the x-y and y-z planes when the GST is amorphous and crystalline. It reveals a significant reduction in the waveguide transmission when the GST changes from the amorphous state to the crystalline state.

The fabricated process flow is described in the Supplementary materials. Fig. 2 shows the overall and magnified images of a typical device after fabrication. The GST sandwiched between the two electrodes has a size of D_{GST} = 1 μm.

We established a comprehensive 2-D finite element (FE) model to study the electro-thermal interactions in our device based on COMSOL Multiphysics. The electric currents and heat transfer in solids modules were coupled via Joule heating and were employed to predict the temperature distribution. Electrically insulating boundary conditions were applied to all external boundaries except for the electrodes. The electrical contact impedance of P⁺⁺-Si/GST photonics, P⁺⁺-Si/Au (~6 × 10⁻¹⁰ Ω m²), and GST/ITO (~1.5 × 10⁻⁹ Ω m²) were set according to the measurement in test structures. The contact resistance measurement is described in the

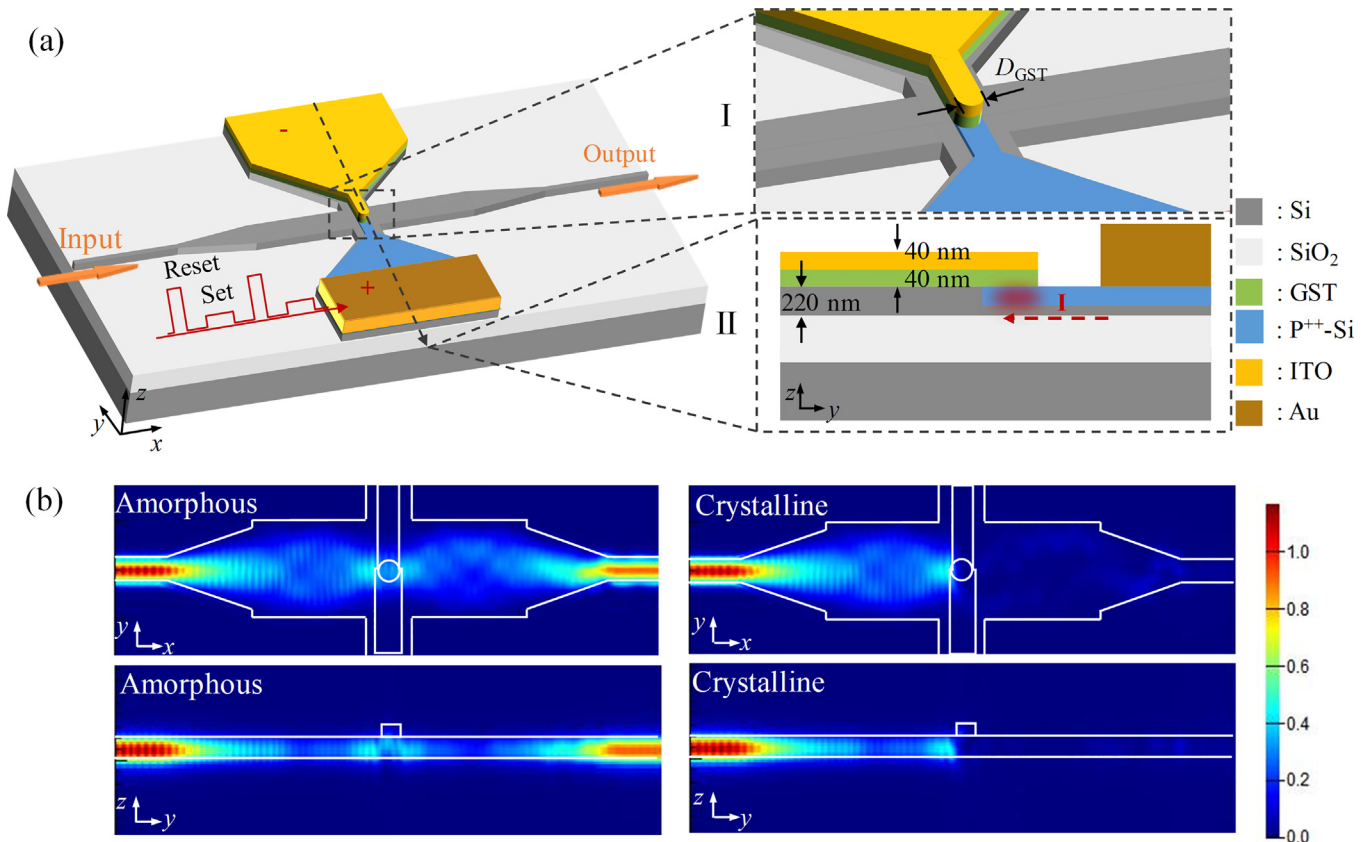


Fig. 1. (Color online) Device structure and optical wave propagation. (a) Schematic structure of the GST-loaded silicon waveguide. The inset I shows the zoom-in view of the active region. The inset II shows the transversal cross-sectional view of the active region. (b) Simulated electric-field intensity distributions through the GST-loaded region when the GST is in amorphous and crystalline states.

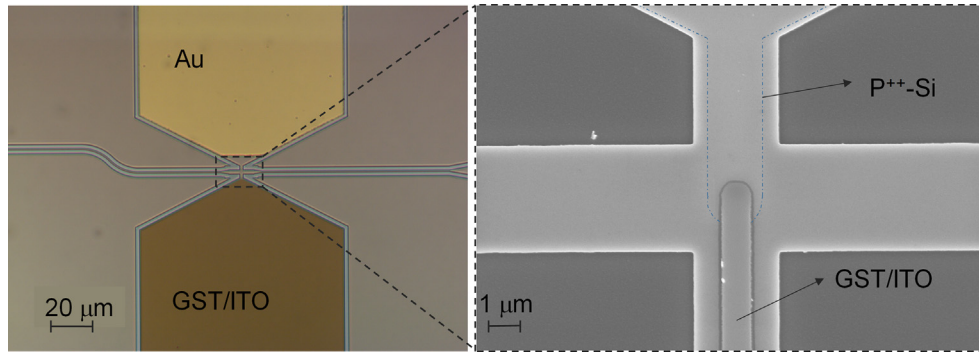


Fig. 2. (Color online) Optical microscope image of the fabricated device. The inset shows the zoom-in scanning electron microscope image of the GST-loaded MMI crossing.

Supplementary material. The thermally insulating boundary conditions were used on all exterior boundaries except for the bottom of the SiO₂, where a constant temperature of $T = 20\text{ }^{\circ}\text{C}$ was assumed (convective cooling by air and radiation cooling are insignificant). **Table 1** summarizes the basic thermal and electrical properties of the materials used in this simulation.

We first simulated the GST crystallization process, corresponding to the transmission change from high to low. The simulation indicates that the temperature rises up to $300\text{ }^{\circ}\text{C}$, when GST is driven by a set pulse with an amplitude of 7 V and a width of 100 ns. It is sufficient to reach the GST crystallization temperature above $250\text{ }^{\circ}\text{C}$ but below the melting point of $650\text{ }^{\circ}\text{C}$. **Fig. 3a** illustrates the temperature change in response to the electrical pulse in the center of the sandwich stack. **Fig. 3c** presents the temperature distribution at the falling edge of the electrical pulse. We next initiated the re-amorphization process, where the GST was heated up to the temperature above its melting point. In the simulation, a reset pulse with an amplitude of 14 V and a width of 20 ns is applied, which raises the temperature above $700\text{ }^{\circ}\text{C}$ in the GST film. **Fig. 3b** shows the temperature distribution in the re-amorphization process. **Fig. 3d** illustrates the corresponding temperature distribution.

3. Experimental results

The experimental setup used for device characterization is described in the **Supplementary material**. **Fig. 4a** shows the transmission spectra for two phase-change cycles (two crystalline states and two amorphous states). The spectra were normalized to a reference straight waveguide. The initial GST was crystalline, presenting a high transmission loss. The re-amorphization of GST was then enabled by using a reset pulse. The transmission loss was reduced from 14 to 7.5 dB at the 1,550 nm wavelength. The heavy-doping induced loss is less than 0.5 dB for the 1- μm -long doping region. Since the amorphization of GST only occurs in the overlapped region, the rest part is still crystalline. This causes a higher loss than expected when the GST is amorphized. Further optimization of the overlap structure can reduce excessive loss. The crystallization of GST was achieved by applying a set pulse, and the transmission returned to the initial higher loss state. These processes can be

repeated with no significant degradation observed. We define the change in transmission as $\Delta T = (T_{\text{am}} - T_{\text{cr}})/T_{\text{cr}}$, where T_{am} and T_{cr} are the transmissivities when the GST of the overlapped region is in the completely amorphous and crystalline states, respectively [24]. It can be seen that ΔT is larger than 300% for the 1- μm -length GST. In fact, there is a compromise between the transmission loss at the amorphous state (T_{am}) and the change in transmission (ΔT). As shown in **Fig. 4b**, the 0.5- μm -long GST has a lower transmission loss of 1.5 dB but the change in the transmission is also reduced down to 52%.

We next investigated the temporal response of the output transmission upon phase change. The probe light was fixed at 1,550 nm. **Fig. 5a** shows the change in transmission upon repeated switching between the crystalline and amorphous states of the GST. The results demonstrate good reversibility and high transmission contrast of our electrically-driven GST. The transmission can be maintained without any electrical current applied, exhibiting a good “self-holding” feature. The inset shows the enlarged view of the electrical driving pulse and the corresponding optical transmission change. The optical waveform is more complex as compared with the electrical one. There co-exist several effects such as phase-change, free-carrier generation, and thermo-optic effects that are all induced by the electrical pulses [18]. For the response with the reset pulse (amorphization process), the transmission change is abrupt after the electrical pulse, resulted from all effects. For the response with the set pulse (crystallization process), two down-stairs were observed. The crystallization process at the first stair was accomplished in 50 ns. The first down-stair represents the phase transition from the amorphous state to the metastable crystalline state with a face-centered cubic structure. The second down-stair represents the phase transition from the metastable crystalline state to the stable crystalline state with a hexagonal structure. **Fig. 5b** shows that the performance of the device is degraded after 1,500 switching cycles.

Our electrically-driven GST element cannot only realize binary switching but is also capable of multi-level switching by controlling the degree of crystallization. **Fig. 5c** shows the optical transmission dynamics in response to a sequence of set and reset pump pulses. Multiple distinguishable intermediate levels are

Table 1
Basic material properties.

Material	Heat capacity (J/(kg K))	Thermal conductivity (W/(m K))	Electrical Conductivity (S/m)	Density (kg/m ³)
Si	720	149	100	2,330
SiO ₂	740	1.38	10^{-14}	2,200
ITO	340	11	8.3×10^3	7,100
GST	210	*Ref. [26]	*Ref. [26]	6,150
Au	129	310	4.4×10^7	19,500

* The thermal and electrical conductivities of GST are not constant.

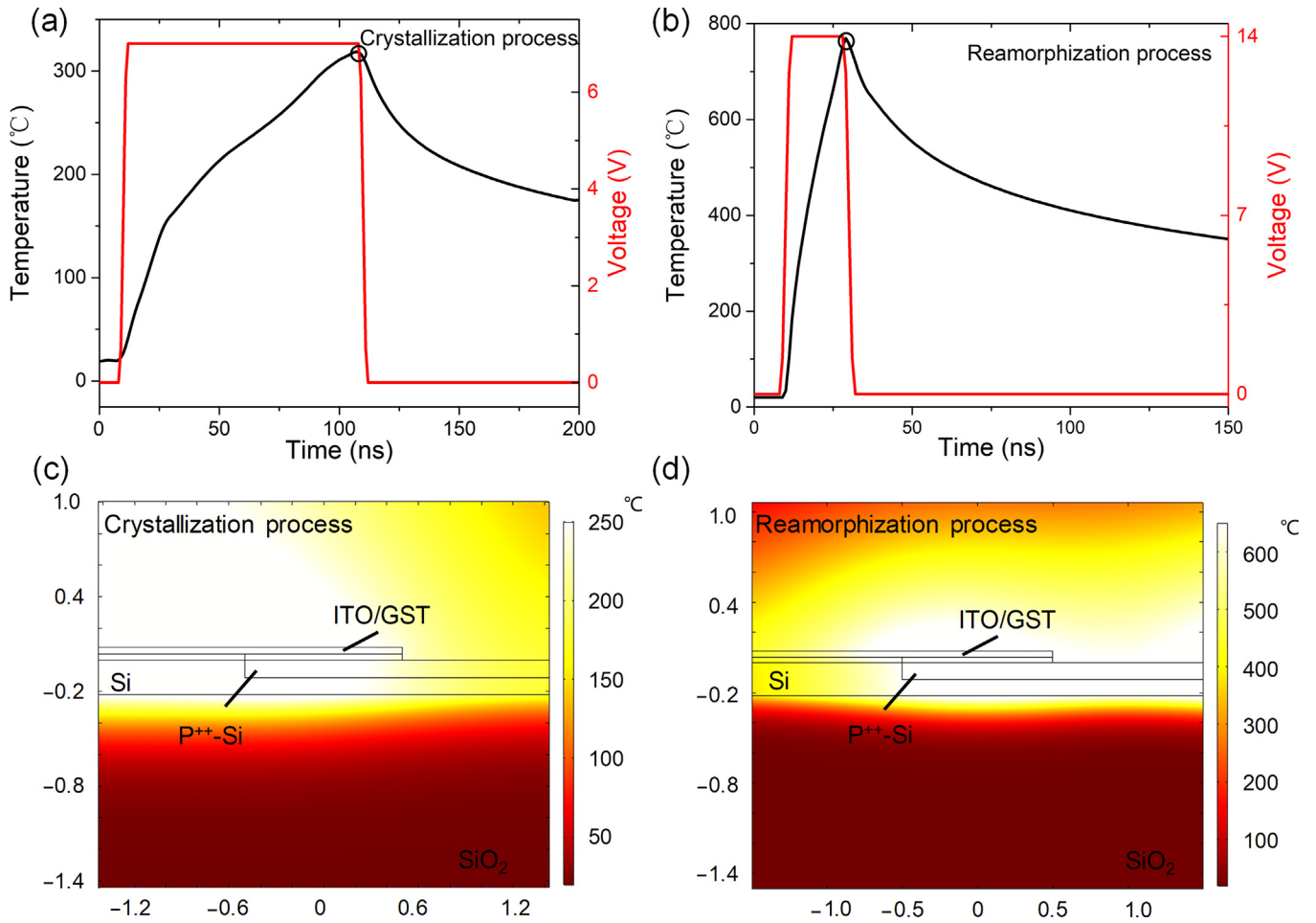


Fig. 3. (Color online) Dynamic thermal process. (a, b) Transient response of the temperature in the center of the P⁺⁺-Si/GST/ITO sandwich stack for (a) the crystallization process and (b) the re-amorphization process. (c, d) Temperature distributions in the device cross-section at the end of the electrical pulses during (c) the crystallization process and (d) the re-amorphization process.

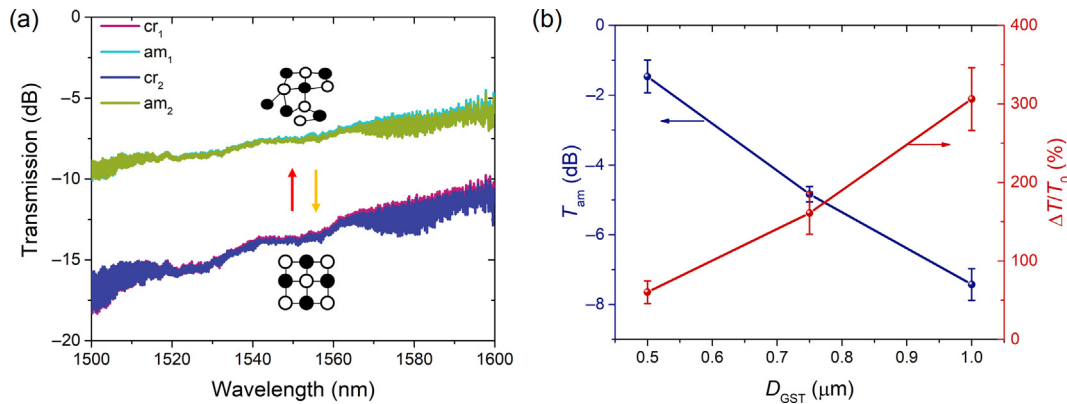


Fig. 4. (Color online) Transmission contrast. (a) Measured transmission spectra of the waveguide over two phase-change cycles. (b) Transmission at the amorphous state and change in transmission between the crystalline and amorphous states for three different GST lengths.

obtained due to the partial crystallization of GST. The initial phase of GST is crystalline with low transmission (level 0). It returns to the high level (level 5) after amorphization at time t_1 using a single reset pulse with a width of 20 ns and an amplitude of 14 V. Three-level partial crystallization of GST is obtained from t_2 to t_3 by using a group of three set pulses. The period, width, and amplitude of the partial crystalline pulses are 100 ms, 50 ns, and 5.2 V, respectively. The transmission returns to the high level (level 5) after

re-amorphization using a single reset pulse with a width of 20 ns and an amplitude of 14 V. The intermediate level (level 1) after a group of three set pulses can further go down to level 0 upon complete crystallization using a set pulse with a width of 100 ns and an amplitude of 7 V as it occurs at t_7 . The transmission can also drop from other levels (level 4, 3 and 2) to level 0 by using a set pulse (t_{14} , t_{19} and t_{12}). We use the color-coded background to mark the difference between the transmissions of any two consecutive

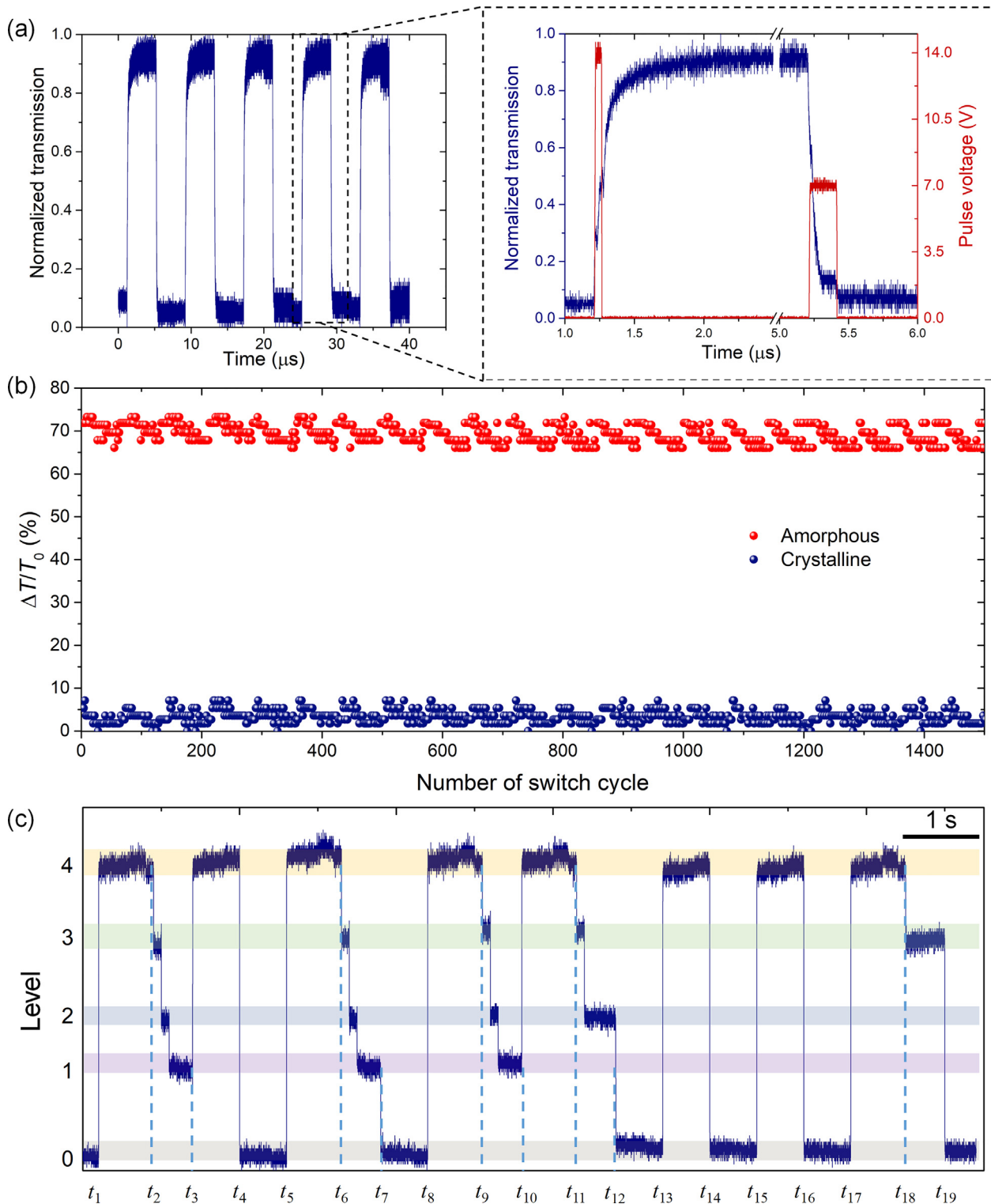


Fig. 5. (Color online) Switching performances. (a) Temporal response of the device with the 1- μm -long GST changed between amorphous and crystalline states. The inset shows the enlarged view of the driving electrical pulses and the resulting optical waveform. (b) Transmission contrast over more than 1,500 switching cycles. (c) Multi-level switching operation of the device showing the dynamic response to a sequence of set and reset pulses.

levels. These exciting results of our electrically-driven GST-enabled switch demonstrate that both set and reset operations, to and from any intermediate level, are possible with accurate control of the transmission levels and remarkable repeatability, just by applying the appropriate set or reset electrical pulses. The number of levels

is mainly limited by the noise of the photodetector. Further reduction of the crystallization pulse power can give more levels. However, the photodetector noise may make it difficult to distinguish two closely-spaced levels. A low-noise photodetector can help obtain more levels.

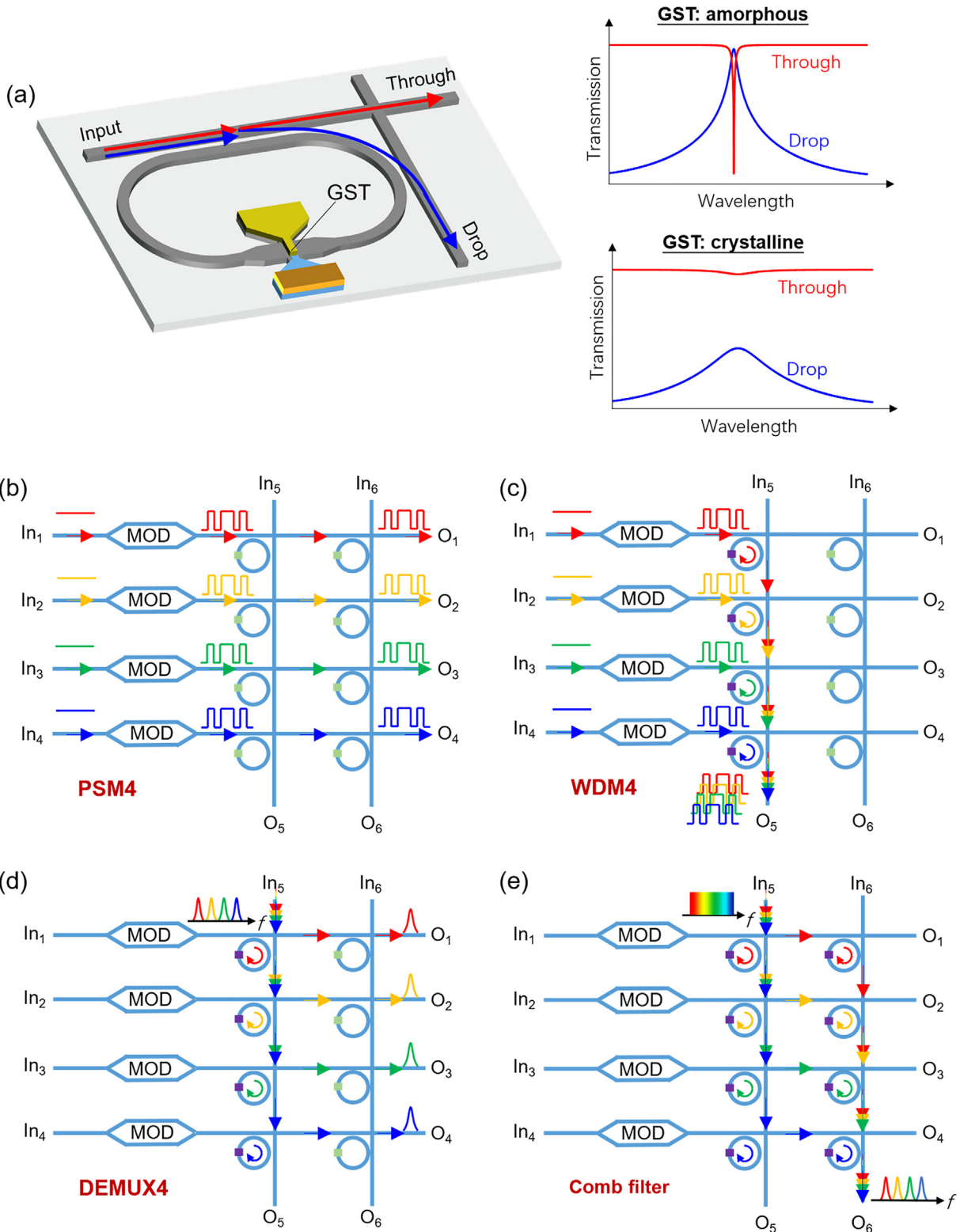


Fig. 6. (Color online) Conceived reconfigurable photonic circuit. (a) Schematic diagram of a 2×2 optical switch composed of a waveguide crossing coupled with a silicon microring resonator. Light at the resonance wavelengths can be switched between the through and drop ports, dependent on the phase state of GST. (b–e) Illustration of a reconfigurable photonic circuit that can be programmed for multiple functions: (b) PSM4 transmitter, (c) WDM4 transmitter, (d) de-multiplexer, and (e) comb filter.

4. Application in reconfigurable photonic circuits

As shown in the [Supplementary material](#), the optical wave suffers a much larger change in amplitude than phase when GST phase change occurs. A new optical phase change material Ge₂Sb₂Se₄Te₁ [27], which exhibits significantly reduced optical

attenuation compared to GST at the 1,550 nm wavelength and a remarkable difference in the real part of refractive index ($\Delta n = 1.5$), could be explored in the future work to get a larger optical phase variation with a lower loss. Nevertheless, it is still possible to build a tunable coupler by varying the optical attenuation, although its tuning range is limited compared to the phase

tuning coupler. Fig. 6a shows an example of the 2×2 tunable coupler consisting of a waveguide crossing coupled with a silicon microring resonator. The GST material is deposited on the ring waveguide to control the internal loss of the resonator. When GST is in the amorphous state, the internal loss is small. As a result, light can resonate in the microring resonator and is finally transmitted to the drop port. With proper design, the critical coupling can be achieved, allowing for the complete elimination of light from the through port at the resonant wavelength. On the other hand, when GST is in the crystalline state, the internal loss increases considerably, destroying the resonances. The input light thus travels to the through port. Therefore, upon phase change of GST, light from the input port can be switched between the through port and the drop port. Variable optical power splitting between these two ports can be achieved by partial crystallization of GST.

With this resonator-assisted tunable coupler, we conceive a silicon photonic chip that can be reconfigured to various functions, as shown in Fig. 6b–e. For example, if we keep all GSTs in the crystalline state, the input light from In_{1-4} will be modulated and guided to O_{1-4} , respectively. It thus forms a parallel single mode (PSM4) transmitter (Fig. 6b). If we keep all GSTs in the amorphous state, the input light from In_{1-4} will be modulated and multiplexed to O_5 . Hence, it becomes a wavelength-division-multiplexer (WDM4) transmitter (Fig. 6c). Making use of the microring resonator cross-bar structure, we can achieve passive signal processing functions such as wavelength demultiplexing (Fig. 6d) and comb filtering (Fig. 6e).

5. Conclusions

We have demonstrated the non-volatile optical transmission control in a GST-clad silicon waveguide. The active region is formed by a stack of P^{++} -Si/GST/ITO films. Electrical pulses applied to the stack can repeatedly change the phase state of GST. The static measurement suggests that the device can operate over a bandwidth of more than 100 nm (limited by measurement) and the transmission change can be >300% for 1- μ m-long GST. The temporal response measurements show that the transmission can be tuned in a controllable and repeatable manner. In particular, multiple intermediate transmission levels can be obtained by partial crystallization of GST. This successful implementation of a tunable silicon waveguide actuated by electrically-driven GST marks a significant step forward in low-power and rewritable optical circuits.

Conflict of interest

The authors declare that they have no conflict of interest.

Acknowledgments

This work was supported by the National Natural Science Foundation of China (61535006, 61705129 and 61661130155), and Shanghai Municipal Science and Technology Major Project (2017SHZDZX03). The authors also thank the Center for Advanced Electronic Materials and Devices (AEMD) of Shanghai Jiao Tong University (SJTU) for the support in device fabrications.

Author contributions

H.Z. designed the devices. H.Z. and J.X. performed material characterization and device fabrication. H.Z., N.W., and H.H. performed

measurements and data analysis. H.Z. and L.Z. discussed and performed theoretical analysis and simulations. L.Z. and L.L. conceived and led the project. B.M.A.R. and J.C. supported and supervised the research. All authors contributed to technical discussions and writing the paper.

Appendix A. Supplementary data

Supplementary data to this article can be found online at <https://doi.org/10.1016/j.scib.2019.04.035>.

References

- [1] Heck MJR, Bauters JF, Davenport ML, et al. Hybrid silicon photonic integrated circuit technology. *IEEE J Sel Top Quant* 2013;19:6100117.
- [2] Wang J, Long Y. On-chip silicon photonic signaling and processing: a review. *Sci Bull* 2018;63:1267–310.
- [3] Wang J. Chip-scale optical interconnects and optical data processing using silicon photonic devices. *Photon Netw Commun* 2016;31:353–72.
- [4] Zhuang L, Roeloffzen CGH, Hoekman M, et al. Programmable photonic signal processor chip for radiofrequency applications. *Optica* 2015;2:854–9.
- [5] Capmany J, Gasulla I, Pérez D. The programmable processor. *Nat Photon* 2015;10:6.
- [6] Anonymous. Birth of the programmable optical chip. *Nat Photon* 2015;10:1.
- [7] Guo Z, Lu L, Zhou L, et al. 16×16 silicon optical switch based on dual-ring-assisted Mach-Zehnder interferometers. *J Lightwave Technol* 2018;36:225–32.
- [8] Lu L, Shen L, Zhou L, et al. Reconfigurable silicon photonic signal processor based on the scow resonant structure. Proceedings of the conference on lasers and electro-optics, San Jose, California, 2018/05/13. Optical Society of America; 2018.
- [9] Wang J, Huang H, Wang X, et al. Reconfigurable 2.3-tbit/s dqpsk simultaneous add/drop, data exchange and equalization using double-pass lcos and bidirectional hnlf. *Opt Express* 2011;19:18246–52.
- [10] Miller KJ, Haglund RF, Weiss SM. Optical phase change materials in integrated silicon photonic devices: review. *Opt Mater Express* 2018;8:2415–29.
- [11] Miller KJ, Hallman KA, Haglund RF, et al. Silicon waveguide optical switch with embedded phase change material. *Opt Express* 2017;25:26527–36.
- [12] Wuttig M, Bhaskaran H, Taubner T. Phase-change materials for non-volatile photonic applications. *Nat Photon* 2017;11:465–76.
- [13] Xu P, Zheng J, Doyle JK, et al. Low-loss and broadband nonvolatile phase-change directional coupler switches. *ACS Photon* 2019;6:553–7.
- [14] Zheng J, Khanolkar A, Xu P, et al. Gst-on-silicon hybrid nanophotonic integrated circuits: a non-volatile quasi-continuously reprogrammable platform. *Opt Mater Express* 2018;8:1551.
- [15] Qu Y, Li Q, Cai L, et al. Polarization switching of thermal emissions based on plasmonic structures incorporating phase-changing material $Ge_2Sb_2Te_5$. *Opt Mater Express* 2018;8:2312–20.
- [16] Kato K, Kuwahara M, Kawashima H, et al. Current-driven phase-change optical gate switch using indium-tin-oxide heater. *Appl Phys Express* 2017;10:072201.
- [17] Stegmaier M, Ríos C, Bhaskaran H, et al. Thermo-optical effect in phase-change nanophotonics. *ACS Photon* 2016;3:828–35.
- [18] Tanaka D, Shoji Y, Kuwahara M, et al. Ultra-small, self-holding, optical gate switch using $ge_2sb_2te_5$ with a multi-mode Si waveguide. *Opt Express* 2012;20:10283–94.
- [19] Zhang H, Zhou L, Xu J, et al. All-optical non-volatile tuning of an amzi-coupled ring resonator with gst phase-change material. *Opt Lett* 2018;43:5539–42.
- [20] von Keitz J, Feldmann J, Gruhler N, et al. Reconfigurable nanophotonic cavities with nonvolatile response. *ACS Photon* 2018;5:4644–9.
- [21] Zhang W, Mazzeo R, Wuttig M, et al. Designing crystallization in phase-change materials for universal memory and neuro-inspired computing. *Nat Rev Mater* 2019.
- [22] Chakraborty I, Saha G, Sengupta A, et al. Toward fast neural computing using all-photonic phase change spiking neurons. *Sci Rep* 2018;8:12980.
- [23] Cheng Z, Ríos C, Pernice WHP, et al. On-chip photonic synapse. *Sci Adv* 2017;3:e1700160.
- [24] Ríos C, Stegmaier M, Hosseini P, et al. Integrated all-photonic non-volatile multi-level memory. *Nat Photon* 2015;9:725–32.
- [25] Hosseini P, Wright CD, Bhaskaran H. An optoelectronic framework enabled by low-dimensional phase-change films. *Nature* 2014;511:206–11.
- [26] Xiong F, Liao AD, Estrada D, et al. Low-power switching of phase-change materials with carbon nanotube electrodes. *Science* 2011;332:568–70.
- [27] Zhang Q, Zhang Y, Li J, et al. Broadband nonvolatile photonic switching based on optical phase change materials: beyond the classical figure-of-merit. *Opt Lett* 2018;43:94–7.



Hanyu Zhang received the B.S. degree in microelectronic manufacturing engineering from Central South University in 2015. She is currently a Ph.D. candidate at the College of Electronic Information and Electrical Engineering, Shanghai Jiao Tong University. Her research concentrates on hybrid integration of phase change materials with silicon photonics for optoelectronic or all-optical applications, such as all-optical synapse, all-optical switch and optical memristive switch.



Linjie Zhou received his Ph.D. degree in electronic and computer engineering from the Hong Kong University of Science and Technology in 2007. From 2007 to 2009, he worked as a postdoctoral researcher at University of California, Davis. Currently, he is a professor in the State Key Laboratory of Advanced Optical Communication Systems and Networks of Shanghai Jiao Tong University. His research interests include silicon photonics and optical integration.